

# Spatial Temporal Transformer Network for Skeleton-based Action Recognition

Chiara Plizzari  
Politecnico di Milano, Italy  
chiara.plizzari@mail.polimi.it

Marco Cannici  
Politecnico di Milano, Italy  
marco.cannici@polimi.it

Matteo Matteucci  
Politecnico di Milano, Italy  
matteo.matteucci@polimi.it

**Abstract**—Skeleton-based Human Activity Recognition has achieved a great interest in recent years, as skeleton data has been demonstrated to be robust to illumination changes, body scales, dynamic camera views and complex background. In particular, Spatial-Temporal Graph Convolutional Networks (ST-GCN) demonstrated to be effective in learning both spatial and temporal dependencies on non-Euclidean data such as skeleton graphs. Nevertheless, an effective encoding of the latent information underlying the 3D skeleton is still an open problem, especially how to extract effective information from joint motion patterns and their correlations. In this work, we propose a novel Spatial-Temporal Transformer network (ST-TR) which models dependencies between joints using the Transformer *self-attention* operator. In our ST-TR model a Spatial Self-Attention module (SSA) is used to understand intra-frame interactions between different body parts, and a Temporal Self-Attention module (TSA) to model inter-frame correlations. The two are combined in a two-stream network, whose performance is evaluated on three large-scale datasets, NTU-RGB+D 60, NTU-RGB+D 120 and Kinetics Skeleton 400, outperforming the state-of-the-art on NTU-RGB+D w.r.t. models using the same input data consisting of joint information.

**Index Terms**—Graph, Transformer, Self-Attention, 3D Skeleton, Action Recognition

## I. INTRODUCTION

Human Action Recognition is achieving increasing interest in recent years, either for the progresses achieved via deep learning and computer vision and for the interest of its applications in human-computer interaction, eldercare and healthcare assistance, and video surveillance. Moreover, recent advances in 3D depth cameras such as Microsoft Kinect sensors [1], [2] and advanced human pose estimation algorithms [3], [4] made it possible to estimate 3D skeleton coordinates quickly and accurately with cheap devices.

Nevertheless, several aspects of skeleton-based action recognition still remain open [5]–[7]. In recent years, the most widespread method to perform skeleton-based action recognition has become Graph Neural Networks (GNNs), and in particular Graph Convolutional Networks (GCNs) since, being an efficient representation of non-Euclidean data, they are able to effectively capture spatial (intra-frame) and temporal (inter-frame) information. Models making use of GCN were first introduced by Yan et al. [8] and they are usually referred to as Spatial-Temporal Graph Convolutional Networks (ST-GCNs). These models process spatial information by operating on bone-connections in the human body along space, and temporal information by considering additional time-connections

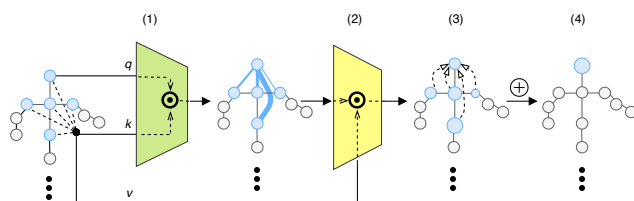


Fig. 1. Self-attention on skeleton joints. (1) For each body joint, a query  $q$ , a key  $k$  and a value vector  $v$  are calculated. Then, the dot product ( $\odot$ ) between the query of the joint and the key of all the other nodes is performed. (2) The results represent the strength of the connection between each pair of nodes. (3) Each node is scaled w.r.t. how it is relevant for the node under consideration. (4) whose new feature is obtained summing the weighted nodes together.

between each joint along time. Despite being proven to perform very well on skeleton data, ST-GCN models have some structural limitations, some of them already addressed in [9]–[12]: (i) The topology of the graph representing the human body is fixed for all layers and all the actions. This may prevent the extraction of rich representations for the skeleton movements during time, especially if graph links are directed and information can only flow along a predefined path. (ii) Both Spatial and Temporal Convolution are implemented starting from a standard 2D convolution. As such, they are limited to operate on a local neighborhood, somehow restricted by the convolution kernel size. (iii) As a consequence of (i) and (ii), correlations between body joints not linked in human skeleton, e.g., the left and right hands, are underestimated even if relevant in actions such as “clapping”. In this paper we face all these limitations by employing a modified Transformer self-attention operator as depicted in Figure 1. Despite being originally designed for Natural Language Processing (NLP) tasks, the sequentiality and hierarchical structure of human skeleton sequences, as well as the flexibility of the Transformer self-attention [13] in modelling long-range dependencies, make this model a perfect solution to tackle ST-GCN weaknesses. Recently, Bello et al. in [14] employed self-attention to overcome the locality of the convolution operator by capturing the global context between the pixels in an image. In our work we aim to apply the same mechanism to spatial-temporal skeleton-based architectures, and in particular to joints representing the human skeleton, with the goal of modeling long range interactions within human actions both in space, through a Spatial Self-Attention module (SSA), and time, through a

Temporal Self-Attention module (TSA) module. Authors of [15] also proposed a Self-Attention Network (SAN) to extract long-term semantic information; however, since it focuses on temporally segmented clips, it solves the locality limitations of convolution only partially.

Contributions of this paper are summarized as follows:

- We propose a novel two-stream Transformer-based model for skeleton activity recognition tasks, employing *self-attention* on both Spatial and Temporal dimension
- We design a *Spatial Self-Attention* (SSA) module to dynamically build links between skeleton joints, representing the relationships between human body parts, conditionally on the action and independently from the natural human body structure. On temporal dimension, we introduce a *Temporal Self-Attention* (TSA) module to study the dynamics of a joint along time <sup>1</sup>
- Our model outperforms ST-GCN [8] and A-GCN [16] baselines on all datasets, and outperforms previous state-of-the-art methods using the same input data on NTU.

## II. RELATED WORKS

### A. Skeleton-based Action Recognition

Most of the early studies in skeleton-based action recognition relied on handcrafted features [17]–[19] exploiting relative 3D rotations and translations between joints. Deep learning revolutionized activity recognition by proposing methods capable of an increased robustness [20] and able to achieve unprecedented performance. Methods that fall into this category rely on different aspects of skeleton data: (1) RNN-based methods [21]–[24] leverage on the sequentiality of joint coordinates, treating input skeleton data as time series. (2) CNN-based methods [25]–[29] leverage on spatial information, in a complementary way to RNN-based ones. Indeed, 3D skeleton sequences are mapped into a pseudo-image, representing temporal dynamics and skeleton joints respectively in rows and columns. (3) GNN-based methods [8], [9], [16], make use of both spatial and temporal data by exploiting information contained in the natural topological graph structure of the human skeleton. These methods have demonstrated to be the most expressive among the three, and among these, the first model capturing the balance between space and temporal dependencies has been the Spatio-Temporal Graph Convolutional Network (ST-GCN) [8]. In ST-GCN the human skeleton is represented as a graph where joints are encoded as nodes and bones as arcs, while time is modeled with additional edges linking together the same joint along time. In this work we used ST-GCNs as baseline model.

### B. Graph Neural Networks

*Geometric deep learning* [30] refers to all emerging techniques attempting to generalize deep learning models to non-Euclidean domains such as graphs. The notion of Graph Neural Network (GNN) was initially outlined in Gori et al. [31] and further elaborated by Scarselli et al. [32]. The intuitive

idea underlying GNNs is that nodes in a graph represent objects or concepts while edges represent their relationships. Due to the success of Convolutional Neural Networks, the concept of convolution has later been generalized from grid to graph data. GNNs iteratively process the graph, each time representing nodes as the result of applying a transformation to nodes' and their neighbors' features. The first formulation of CNNs on graphs is due to Bruna et al. [33], who generalized convolution to signals using a *spectral* construction. This approach had computational drawbacks that have been subsequently addressed by Henaff et al. [34] and Defferrard et al. [35]. The latter has been later simplified and extended by Kipf et al. [36]. Another approach is the *spatial* one, where graph convolution is defined as information aggregation [37]–[39]. This work is based on the method of [36].

### C. Transformer

The Transformer is the leading neural model for Natural Language Processing (NLP), proposed by Vaswani et al. [13] as an alternative to recurrent networks. It has been designed to face two key problems: (i) the processing of very long sequences, which are often intractable both for LSTMs and RNNs, and (ii) limitations in parallelizing sentence processing, which is usually performed word by word in standard RNNs architectures. The Transformer follows the usual encoder-decoder structure, but it relies solely on *multi-head self-attention*. Recently, self-attention mechanisms have been also applied to visual tasks by Bello et al. [14], with the purpose of augmenting standard convolution. Our work is one of the few in literature applying self-attention on graphs [40].

## III. BACKGROUND

### A. Spatial Temporal Graph Convolutional Networks

Spatial Temporal Graph Convolutional Networks (ST-GCN) have been introduced by Yan et al. [8]. A ST-GCN is structured as a hierarchy of stacked spatial-temporal blocks, which are internally composed of a spatial convolution (GCN) followed by a temporal convolution (TCN). The spatial sub-module uses the Graph Convolution formulation proposed by Kipf and Welling [36], which can be summarized as it follows:

$$\mathbf{f}_{out} = \sum_k^{K_s} (\mathbf{f}_{in} \mathbf{A}_k) \mathbf{W}_k \quad (1)$$

$$\mathbf{A}_k = \mathbf{D}_k^{-\frac{1}{2}} (\tilde{\mathbf{A}}_k + \mathbf{I}) \mathbf{D}_k^{-\frac{1}{2}}, \mathbf{D}_{ii} = \sum_k^{K_s} (\tilde{\mathbf{A}}_k^{ij} + \mathbf{I}_{ij}) \quad (2)$$

where  $K_s$  is the kernel size on spatial dimension,  $\tilde{\mathbf{A}}_k$  is the adjacency matrix of the undirected graph representing intra-body connections,  $\mathbf{I}$  is the identity matrix and  $\mathbf{W}_k$  is a trainable weight matrix. The temporal convolution sub-module (TCN) is implemented as a  $1 \times K_t$  standard 2D convolution operating on  $(V, T)$  dimensions of the  $(C_{in}, V, T)$  input volume, where  $K_t$  is the number of frames considered within the kernel receptive field. As shown in Equation 1, the graph structure is predefined, being the adjacency matrix fixed. In order to make

<sup>1</sup>Code at <https://github.com/Chiarapizz/ST-TR>

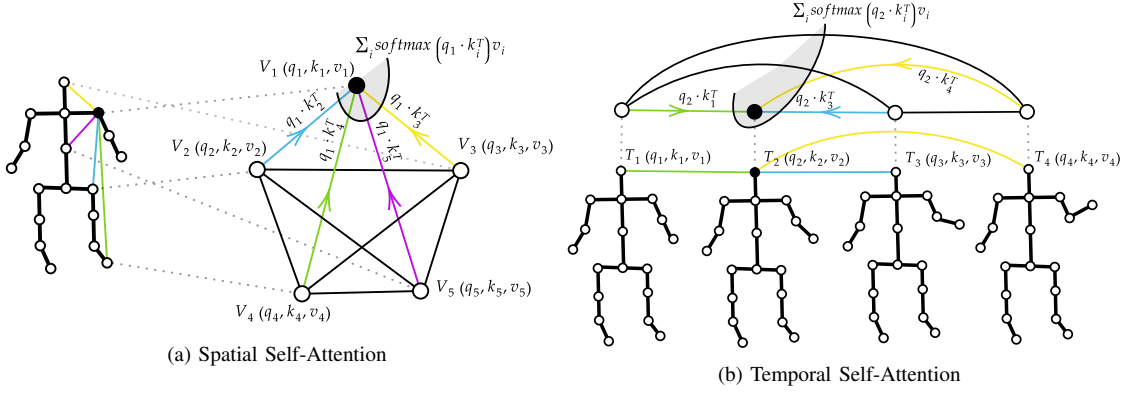


Fig. 2. Spatial Self-Attention (SSA) and Temporal Self-Attention (TSA). Self-attention operates on each pair of nodes, by computing a weight for each of them which represents the strength of their correlation. Those weights are then used to score the contribution of each body joint  $V_i$  (in the case of SSA) or the contribution of each time frame  $T_i$  (in the case of TSA), proportionally to how relevant the node is w.r.t. to all the others. Please notice that on SSA (a), the procedure is illustrated only of a group of five nodes for simplicity, while in practice it operates on all the nodes.

it *adaptive*, the authors of [16] introduced the *Adaptive Graph Convolutional Network* (A-GCN), where the GCN formulation in Equation 1 is changed with the following:

$$\mathbf{f}_{out} = \sum_k^{K_s} \mathbf{f}_{in} (\mathbf{A}_k + \mathbf{B}_k + \mathbf{C}_k) \mathbf{W}_k \quad (3)$$

where  $\mathbf{A}_k$  is the same as the one in Equation 1,  $\mathbf{B}_k$  is learned during training, and  $\mathbf{C}_k$  determines whether two vertices are connected or not through a similarity function.

### B. Transformer Self-Attention

The Transformer model of Vaswani et al. [13] employs *self-attention*, i.e., a *non-local operator* originally designed to operate on word embeddings in NLP tasks. For each word embedding, a query  $\mathbf{q} \in \mathbb{R}^{d_q}$ , a key  $\mathbf{k} \in \mathbb{R}^{d_k}$  and a value vector  $\mathbf{v} \in \mathbb{R}^{d_v}$  are computed through trainable linear transformations. A score for each word embedding  $\mathbf{w}_i \in W = \{\mathbf{w}_1, \dots, \mathbf{w}_n\}$  is obtained by taking the dot product  $\mathbf{q}_i \cdot \mathbf{k}_j^T \forall i, j = 1, \dots, n$ . The score represents how much the word  $j$  is relevant for word  $i$ , and it is used to weight the value vector  $\mathbf{v}_i$ . This process, also called *scaled dot-product attention*, can be written in matrix form as it follows:

$$Attention(\mathbf{Q}, \mathbf{K}, \mathbf{V}) = softmax \left( \frac{\mathbf{QK}^T}{\sqrt{d_k}} \right) \mathbf{V} \quad (4)$$

where  $\mathbf{Q}$ ,  $\mathbf{K}$ , and  $\mathbf{V}$  are the matrices containing all query, key and value vectors respectively packed together and  $d_k$  is the channel dimension of the key vectors. The division by  $\sqrt{d_k}$  is performed in order to increase gradients stability during training. In order to obtain better performance, a mechanism called *multi-headed attention* is usually applied, which consists in applying attention, i.e., a head, multiple times with different learnable parameters and then finally combining the results.

## IV. SPATIAL TEMPORAL TRANSFORMER NETWORK

We propose an architecture called *Spatial Temporal Transformer* (ST-TR) which uses the Transformer self-attention

mechanism to operate on both space and time dimensions. We propose to achieve this goal using two novel modules, one called *Spatial Self-Attention module* (SSA) and one called *Temporal Self-Attention module* (TSA), each one focusing on extracting correlations on one of the two dimensions.

### A. Spatial Self-Attention (SSA)

The Spatial Self-Attention module applies self-attention inside each frame, i.e., computing correlations between each pair of joints in each single frame independently, as depicted in Figure 2-a. SSA is computed in parallel on  $h$  attention heads. Each attention head takes as input a sequence of  $\mathbf{n} = (\mathbf{n}_1^t, \dots, \mathbf{n}_{N_v}^t)$  nodes,  $\mathbf{n}_i^t \in \mathbb{R}^{C_{in}}$  and  $C_{in}$  being the number of input channels, for each  $t \in T = \{1, \dots, F\}$  frames, being  $F$  is the total number of frames. The result of SSA is a sequence  $\mathbf{z} = (\mathbf{z}_1^t, \dots, \mathbf{z}_{N_v}^t)$  of  $N_v$  embeddings, where  $\mathbf{z}_i^t \in \mathbb{R}^{C_{out}}$  (being  $C_{out}$  the number of output channels) is associated to node  $\mathbf{n}_i$ , and weighted according to its relevance in the sequence.

First, for each node  $\mathbf{n}_i^t$  a *query*  $\mathbf{q}_i^t \in \mathbb{R}^{d_{qn}}$ , a *key*  $\mathbf{k}_i^t \in \mathbb{R}^{d_{kn}}$  and a *value* vector  $\mathbf{v}_i^t \in \mathbb{R}^{d_{vn}}$  are calculated. Then, for each pair of body nodes  $(\mathbf{n}_i^t, \mathbf{n}_j^t)$ , a *query-key dot product* is applied to obtain a weight  $\alpha_{ij} \in \mathbb{R}$  representing the strength of the correlations between the two body joints, as expressed in the following:

$$\alpha_{ij}^t = \mathbf{q}_i^t \cdot \mathbf{k}_j^{tT}, \forall t \in T \quad (5)$$

The resulting score  $\alpha_{ij}^t$  is used to weight each joint value  $\mathbf{v}_j^t$ , and a weighted sum is computed to obtain a global importance of node  $\mathbf{n}_i$  in the sequence, as in the following:

$$\mathbf{z}_i^t = \sum_j softmax_j \left( \frac{\alpha_{ij}^t}{\sqrt{d_k}} \right) \mathbf{v}_j^t \quad (6)$$

where  $\mathbf{z}_i^t$  is the resulting weighted node.

Thus, the relations between nodes are dynamically *predicted* via the SSA module. Moreover, the correlation structure is not fixed for all the actions, but it changes adaptively for each sample. As shown in Figure 2-a, starting from a fully-connected graph connecting all the body nodes, a weighted

graph is obtained according to how relevant are the links between joints. Weights are then used to score the contribution of each node.

### B. Temporal Self-Attention (TSA)

Along the temporal dimension, the dynamics of each joint is studied separately along all the frames, i.e., each single node is considered as independent and correlations between frames are computed by comparing the node features along the temporal dimension. Each Temporal Self-Attention head operates on a sequence  $\mathbf{t} = (\mathbf{t}_1^v, \dots, \mathbf{t}_{N_t}^v)$  of frames,  $\mathbf{t}_i^v \in \mathbb{R}^{C_{in}}$ , being  $C_{in}$  the number of input channels, for each of the  $v \in V = \{1, \dots, V\}$  nodes. The result of TSA is a sequence  $\mathbf{z} = (\mathbf{z}_1^v, \dots, \mathbf{z}_{N_t}^v)$  of  $N_t$  embeddings, where  $\mathbf{z}_i^v \in \mathbb{R}^{C_{out}}$  (being  $C_{out}$  the number of output channels) is associated to each input frame, and weighted according to its relevance in the sequence. The formulation is symmetrical to the one reported in Equations (5) and (6) for SSA:

$$\begin{aligned} \alpha_{ij}^v &= \mathbf{q}_i^v \cdot \mathbf{k}_j^{vT}, \forall v \in V \\ \mathbf{z}_i^v &= \sum_j \text{softmax}_j \left( \frac{\alpha_{ij}^v}{\sqrt{d_k}} \right) \mathbf{v}_j^v \end{aligned} \quad (7)$$

where  $\alpha_{ij}^v \in \mathbb{R}$ ,  $\mathbf{q}_i^v \in \mathbb{R}^{d_{q_h}}$  is the query associated to frame  $\mathbf{t}_i^v$ , and  $\mathbf{k}_j^v \in \mathbb{R}^{d_{k_h}}$  and  $\mathbf{v}_j^v \in \mathbb{R}^{d_{v_h}}$  the key and value associated to frame  $\mathbf{t}_j^v$ , and  $\mathbf{z}_i^v$  is the resulting weighted frame. An illustration of TSA is represented in Figure 2-b. The inter-frame relations between nodes in time are used to extract importance scores of each time frame. In this way, the network can learn to correlate frames apart from each other (e.g., the first frame with the last one), capturing discriminant features that are not otherwise possible to capture with the ST-GCN standard convolution, being this limited by the kernel size.

### C. Implementation of SSA and TSA

The matrix implementation of SSA (and of TSA) is based on the implementation of Transformer on pixels by [14]. As shown in Figure 3, given an input tensor of shape  $(C_{in}, T, V)$ , where  $C_{in}$  is the number of input features,  $T$  is the number of frames and  $V$  is the number of nodes, a matrix  $\mathbf{X}_V \in \mathbb{R}^{C_{in} \times 1 \times V}$  is obtained by reshaping the input. Here the  $T$  dimension is moved inside the batch dimension, effectively implementing parameter sharing along the temporal dimension and applying the transformation separately on each frame:

$$\begin{aligned} \text{head}_i(\mathbf{X}_V) &= \text{Softmax} \left( \frac{(\mathbf{X}_V \mathbf{W}_q)(\mathbf{X}_V \mathbf{W}_k)^T}{\sqrt{d_k^h}} \right) (\mathbf{X}_V \mathbf{W}_v) \\ \text{SelfAttention}_V &= \text{Concat}(\text{head}_1, \dots, \text{head}_h) \mathbf{W}^o \end{aligned} \quad (8)$$

where  $\mathbf{Q}, \mathbf{K}$  and  $\mathbf{V}$  have a shape respectively of  $(N, N_h, V, d_q^h)$ ,  $(N, N_h, V, d_k^h)$  and  $(N, N_h, V, d_v^h)$ , being  $N_h$  the number of heads, and  $\mathbf{W}^o$  is a learnable linear transformation combining the heads outputs. The output of the Spatial Transformer is then reshaped back into  $(N, C_{out}, T, V)$ . The TSA matrix implementation has the same expression as Equation (8), differing only in the way

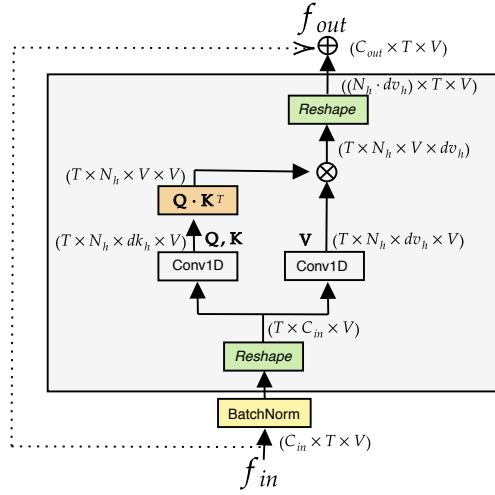


Fig. 3. Illustration of a SSA module (the implementation of TSA is the same, with the only difference that the dimension  $V$  corresponds to  $T$  and viceversa). The input  $f_{in}$  is reshaped by moving  $T$  in the batch dimension, such that self-attention operated on each time frame separately. SSA is implemented as a matrix multiplication, where  $\mathbf{Q}, \mathbf{K}$  and  $\mathbf{V}$  are the query, key and value matrix respectively, and  $\otimes$  denotes the matrix multiplication.

the input  $\mathbf{X}$  is processed. Indeed, in order to be processed by each TSA module, the input is reshaped into a matrix  $\mathbf{X}_T \in \mathbb{R}^{C_{in} \times 1 \times T}$ , where the  $V$  dimension has been moved inside the batch dimension in order to operate separately on each joint along the time dimension. The formulation is the same of the one in Equation (8), where  $\mathbf{Q}, \mathbf{K}$  and  $\mathbf{V}$  have a shape respectively of  $(N, N_h, T, d_q^h)$ ,  $(N, N_h, T, d_k^h)$  and  $(N, N_h, T, d_v^h)$ , being  $N_h$  the number of heads.

### D. Two-Stream Spatial Temporal Transformer Network

In order to properly combine the SSA and TSA modules, a two-stream architecture, named 2s-ST-TR, is used, as similarly proposed by Shi et al. in [16] and [9]. In our formulation, the two streams differentiate on the way the self-attention mechanism is applied: SSA operates on the spatial stream (named S-TR stream), while TSA on the temporal one (named T-TR stream). In both streams, the architecture is composed by 9 layers, of channel dimension 64, 64, 64, 128, 128, 128, 256, 256 and 256. Batch normalization is applied to input coordinates, and a global average pooling layer is applied before the softmax classifier. On both the streams, low level features are extracted through a three-layers residual network, where each layer processes the input on spatial dimension through graph convolution (GCN), and on temporal dimension through a standard 2D convolution (TCN), as in [8]. In the remaining, SSA and TSA are applied on the S-TR and on the T-TR stream in substitution to GCN and TCN respectively. The sub-networks output are finally fused together by summing up their softmax output scores to obtain the final prediction.

**Spatial Transformer Stream (S-TR):** In the spatial stream, self-attention is applied at the skeleton level through a SSA module, which focuses on spatial relations between joints. The output of the SSA module is passed to a 2D

convolutional module with kernel  $K_t$  on temporal dimension (TCN), as in [8], in order to extract temporally relevant features, as shown in Figure 4 and expressed in the following:

$$\mathbf{S-TR}(x) = \text{Conv}_{2D(1 \times K_t)}(\mathbf{SSA}(x)) \quad (9)$$

Following the original Transformer structure, the input is pre-normalized passing through a Batch Normalization layer [41], [42], and skip connections are used to sum the input to the output of the SSA module (see Figure 3).

**Temporal Transformer Stream (T-TR):** The temporal stream, instead, focuses on discovering inter-frame temporal relations. Similarly to the S-TR stream, inside each T-TR layer, a standard graph convolution sub-module [8] is followed by the proposed Temporal Self-Attention module:

$$\mathbf{T-TR}(x) = \mathbf{TSA}(\text{GCN}(x)) \quad (10)$$

In this case, TSA operates on graphs linking the same joint along all the time dimension (e.g., all left feet, or all right hands).

## V. MODEL EVALUATION

To understand the impact of both Spatial Transformer and Temporal Transformer streams, we analyze their performance separately and in different configurations by performing extensive experiments on the NTU-RGB+D 60 [43] dataset (see Table I, II). Then, we test the resulting best configurations on the Kinetics [44] dataset, which are used by most of previous works, and on the NTU-RGB+D 120 [45] dataset, which represents to date one of the most complex skeleton-based action recognition benchmarks, for a comparison with the state-of-the-art (see Table III, Table IV).

### A. Datasets

**NTU RGB+D 60 and NTU RGB+D 120:** The NTU RGB+D 60 (NTU-60) Dataset is a large-scale benchmark for 3D human action recognition collected using Microsoft Kinect v2 by Shahroudy et al. [43]. It contains RGB videos, depth sequences, skeleton data, and infrared frames collected in 56,880 RGB+D video samples. Skeleton information consists of 3D coordinates of 25 body joints, representing a total of 60 different action classes. The NTU-60 dataset follows two different criteria for evaluation. The first one, called *Cross-View Evaluation (X-View)*, is composed of 37,920 training and 18,960 test samples, splitted according to the camera from which the action is taken. The second one, called *Cross-Subject Evaluation (X-Sub)*, is composed instead of 40,320 training and 26,560 test samples. Data collection has been performed with 40 different subjects performing actions and divided into two groups, one for training and the other for testing. NTU RGB+D 120 [45] (NTU-120) is an extension of NTU-60, which adds 57,367 new skeleton sequences representing 60 new actions, for a total of 113,945 videos and 120 classes obtained from 106 subjects and 32 camera setups. In order to perform the evaluation, the extended dataset follows two criteria: the first one is the *Cross-Subject Evaluation (X-Sub)*, the same used for NTU-60, and the second one is called

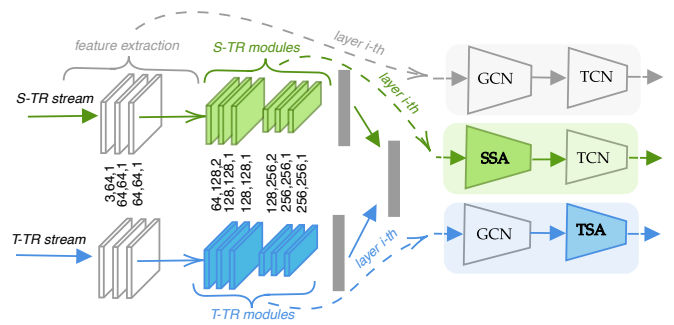


Fig. 4. Illustration of two 2s-ST-TR architecture. On each stream, the first three layers extract low level features. On the S-TR stream, at each layer SSA is used to extract spatial information, followed by a 2D convolution on time dimension (TCN), while on the T-TR stream, at each layer, TSA is used to extract temporal information, while spatial features are extracted by a standard graph convolution (GCN) [8].

*Cross-Setup Evaluation (X-Set)*, which substitutes Cross-View by splitting training and testing samples based on the parity of the camera setup IDs.

**Kinetics:** The Kinetics skeleton dataset [8] is obtained by extracting skeleton annotations from videos composing the Kinetics 400 [44] dataset, by using the OpenPose toolbox [3]. It consists of 240,436 training and 19,796 testing samples, representing a total of 400 action classes. Each skeleton is composed by 18 joints, each one provided with the 2D coordinates and a confidence score. For each frame, a maximum of 2 people are selected based on the highest confidence scores. To compare our methods with the previous ones, Top-1 and Top-5 accuracy are reported.

### B. Experimental Settings

Using Pytorch [46] framework, we trained our models for a total of 120 epochs with batch size 32 and SGD as optimizer on NTU-60 and NTU-120, while on Kinetics we trained our models for a total of 65 epochs, with batch size 128. The learning rate is set to 0.1 at the beginning and then reduced by a factor of 10 at the epochs  $\{60, 90\}$  and  $\{45, 55\}$  for NTU and Kinetics respectively. These schedulings have been proven to provide good results on ST-GCN networks in [9]. Moreover, we preprocessed the data with the same procedure used by Shi et al. in [16] and [9]. In order to avoid overfitting, we also used *DropAttention*, a particular dropout technique introduced by Zehui et al. [47] for regularizing attention weights in Transformer, that consists in randomly dropping columns of the attention logits matrix. In all of these experiments, the *number of heads* for multi-head attention is set to 8, and  $d_q, d_k, d_v$  embedding dimensions to  $0.25 \times C_{out}$  in each layer, as in [14]. We did not performed grid search on these parameters.

### C. Two-stream Spatial Temporal Transformer Attention

To verify in a fair way the effectiveness of our SSA and TSA modules, we compare separately the S-TR stream and T-TR stream against the ST-GCN [8] baseline and other models that

TABLE I

COMPARISON BETWEEN THE BASELINE AND OUR SELF-ATTENTION MODULES IN TERMS OF BOTH PERFORMANCE (ACCURACY (%)) AND EFFICIENCY (NUMBER OF PARAMETERS) ON NTU-60 (X-VIEW)

Method	GCN	TCN	Params $\times 10^5$	Top-1	Method	
					Params $\times 10^4$	Params $\times 10^4$
ST-GCN [8]	✓	✓	31.0	92.7	GCN [8]	19.9
ST-GCN (fc)	$\mathbf{A}_{fc}$	✓	26.5	93.7	SSA	17.8
1s-AGCN [16]	AGCN	✓	34.7	93.7	TCN [8]	59.0
1s-AGCN w/o A [16]	AGCN	✓	33.1	93.4	TSA	17.7
S-TR	SSA	✓	30.7	94.0		
T-TR	✓	TSA	17.6	93.6		

(a)

(b)

modify its basic GCN module (see Table I): (i) *ST-GCN (fc)*: we implemented a version of ST-GCN whose adjacency matrix is composed of all ones (referred as  $\mathbf{A}_{fc}$ ), to simulate the fully-connected skeleton structure underlying our SSA module and verify the superiority of self-attention over graph convolution on the spatial dimension; (ii) *1s-AGCN*: Adaptive Graph Convolutional Network (AGCN) [16] (see Section III-A), as it demonstrated in the literature to be more robust than standard ST-GCN, in order to remark the robustness of our SSA module over more recent methods; (iii) *1s-AGCN w/o A*: 1s-AGCN without the static adjacency matrix, to verify the effectiveness of our SSA over graph convolution in a similar setting where all the links between joints are exclusively learnt. All these methods use the same implementation of convolution on the temporal dimension (TCN). We make a comparison both in terms of model accuracy and number of parameters.

As far as it concerns the SSA, the performance of S-TR is superior to all methods mentioned above, demonstrating that self-attention can be used in place of graph convolution, increasing the network performance while also decreasing the number of parameters. In fact, as it can be seen from Table I-a, S-TR introduces  $0.3 \times 10^5$  parameters less than ST-GCN and  $4 \times 10^5$  less than 1s-AGCN, with an increment in the performance w.r.t. all GCN configurations. Similarly, regarding TSA, what emerges from the comparison between T-TR and the ST-GCN baseline adopting standard convolution, is that by using self-attention on the temporal dimension the model is significantly lighter ( $13.4 \times 10^5$  less parameters), and achieves an increment of accuracy of 0.9%. Table I-b shows the difference in terms of parameters between a single GCN (TCN) and the corresponding SSA (TSA) module, with  $C_{in} = C_{out} = 256$ . Especially on the temporal dimension, TSA results in a decrease in parameters, introducing  $17.7 \times 10^4$  parameters, i.e.,  $41.3 \times 10^4$  less than TCN. Please refer to supplementary material for more details about model complexity.

In Table II we first analyze the performance of the S-TR stream, T-TR stream and their combination by using input data consisting of joint information only. As it can be seen from Table II-a, on NTU-60 the S-TR stream achieves slightly better performance (+0.4%) than the T-TR stream, on both X-View and X-Sub. This can be motivated by the fact that SSA in S-TR operates on 25 joints only, while on temporal

TABLE II

A) COMPARISON OF ACCURACY (%) OF S-TR AND T-TR STREAM, AND THE COMBINATION OF THE TWO (ST-TR) ON NTU-60, W AND W/O BONES. B) ABLATIONS OF DIFFERENT MODEL CONFIGURATIONS

Method	Bones X-Sub X-View		Method	X-View
	X-Sub	X-View		
S-TR	86.4	94.0	S-TR-all-layers	93.3
T-TR	86.0	93.6	T-TR-all-layers	91.3
ST-TR	88.7	95.6	ST-TR-all-layers	95.0
S-TR	✓	87.9	S-TR-augmented	94.5
T-TR	✓	87.3	T-TR-augmented	90.2
T-TR-agcn	✓	86.1	ST-TR-augmented	94.9
ST-TR	✓	89.9	ST-TR-1s	93.3
ST-TR-agcn	✓	89.3		

(a)

(b)

dimension the number of correlations is proportional to the huge number of frames. Again, as shown in Table I-a, applying self-attention instead of convolution clearly benefits the model on both spatial and temporal dimensions. Following [16] and [9], combining the two streams achieves 88.7% of accuracy on X-Sub and 95.6% of accuracy on X-View, surpassing other two-stream architectures, but without making use of bones (see Table IV).

As adding bones information demonstrated to lead to better results in previous works [9], [10], we also studied the effect of our Transformer module on combined joint and bones information. For each node  $\mathbf{v}_1 = (\mathbf{x}_1, \mathbf{y}_1, \mathbf{z}_1)$  and  $\mathbf{v}_2 = (\mathbf{x}_2, \mathbf{y}_2, \mathbf{z}_2)$ , the bone connecting the two is calculated as  $\mathbf{b}_{\mathbf{v}_1, \mathbf{v}_2} = (\mathbf{x}_2 - \mathbf{x}_1, \mathbf{y}_2 - \mathbf{y}_1, \mathbf{z}_2 - \mathbf{z}_1)$ . Joint information and bone information are concatenated along the channel dimension, and then fed to the network. At each layer, the dimension of the input and output channels are doubled as in [9], [10]. The performance results are shown again in Table II-a, where all previous configurations improve when bones information is added as input. This highlights the flexibility of our method, which is capable of adapting to different input types and network configurations.

To further test its flexibility, we also perform additional experiments in which the GCN module is substituted by the AGCN adaptive module on the temporal stream. As it can be seen from Table II-a, these configurations (*T-TR-agcn*) achieve better results than the one using standard GCN (T-TR-agcn: 94.3%, T-TR: 94.1%) on X-View.

#### D. Effect of Applying Self-Attention to Feature Extraction

We designed our streams to operate starting from high-level features, rather than directly from coordinates. This set of experiments validates our design choice. In these experiments SSA (TSA) substitutes GCN (TCN) on the S-TR (T-TR) stream, from the very first layer. The configurations reported in Table II-b (named *S-TR-all-layers*), perform worse than the corresponding ones in Table II-a, while still outperforming the baseline ST-GCN [9] by 2.3% (see Table IV). Notice that on T-TR, in order to deal with the great number of frames in the very first layers ( $T = 300$ ), we divided frames into blocks within which SSA is applied, and then gradually reduce the number of blocks going deeper in the architecture ( $d_{block} = 10$

TABLE III

COMPARISON WITH STATE-OF-THE-ART ACCURACY (%) OF S-TR, T-TR, AND THEIR COMBINATION (ST-TR) ON NTU-120 (A) AND KINETICS (B)

NTU-120			Kinetics			
Method	X-Sub	X-Set	Method	Bones	Top-1	Top-5
ST-LSTM [48]	55.7	57.9	ST-GCN [8]		30.7	52.8
GCA-LSTM [49]	61.2	63.3	2s-AGCN [16]	✓	36.1	58.7
RotClips+MTCNN [50]	62.2	61.8	DGCNN [9]	✓	36.9	59.6
Pose Evol. Map [51]	64.6	66.9	MS-G3D [12]	✓	38.0	60.9
1s Shift-GCN [11]	80.9	83.2	SAN [15]		35.1	55.7
<b>Ours</b>	X-Sub	X-Set	<b>Ours</b>		Top-1	Top-5
S-TR	78.6	80.7	S-TR		32.4	55.3
T-TR	78.4	80.5	T-TR		32.4	55.2
T-TR-agcn	80.3	81.8	ST-TR		34.5	57.6
ST-TR	81.9	84.1	S-TR	✓	35.4	57.9
ST-TR-agcn	<b>82.7</b>	<b>84.7</b>	T-TR-agcn	✓	33.7	55.1
			ST-TR-agcn	✓	<b>37.4</b>	<b>59.8</b>

(a)

(b)

where  $C_{out} = 64$ ,  $d_{block} = 10$  where  $C_{out} = 128$ , and a single block of  $d_{block} = T^l$  on layers  $l$  with  $C_{out} = 256$ ).

### E. Effect of Augmenting Convolution with Self-Attention

Motivated by the results in [14], we studied the effect of applying the proposed Transformer mechanism as an augmentation procedure to the original ST-GCN modules. In this configuration,  $0.75 \times C_{out}$  features result from GCN (TCN) and are concatenated to the remaining  $0.25 \times C_{out}$  features from SSA (TSA), a setup that has proven to be effective in [14]. To compensate the reduction of attention channels, *wide attention* is used, i.e., half of the attention channels are assigned to each head, then recombined together while merging heads (more details in the supplementary materials). The results are reported in Table II-b (referred as *ST-TR-augmented*). Graph convolution is the one that benefits the most from SSA attention (S-TR-augmented, 94.5%), to be compared with S-TR's 94% in Table II-a, obtained by SSA only. Nevertheless, the lower number of output features assigned to self-attention does not improve temporal convolution on T-TR stream.

### F. Effect of combining SSA and TSA on one stream

We test the efficiency of the model when SSA and TSA are combined in a single stream architecture (see Table II-b, referred as *S-TR-1s*). In this configuration, feature extraction is still performed by the original GCN and TCN modules, while from the 4th layer on, each layer is composed by SSA followed by TSA, i.e.,  $\mathbf{ST-TR-1s}(x) = \mathbf{TSA}(\mathbf{SSA}(x))$ .

We test this configuration on NTU-60, obtaining an accuracy of 93.3%, slightly lower than the 95.6% accuracy obtained by the two-stream configuration (see Table I-a, ST-TR). However, it should be noted that this configuration presents  $17.4 \times 10^5$  parameters, drastically reducing the complexity of the baseline ST-GCN which consists in  $31 \times 10^5$  parameters. Nevertheless, it outperforms the baseline by 0.6% by introducing half of the parameters.

TABLE IV

COMPARISON WITH STATE-OF-THE-ART ACCURACY (%) ON NTU-60

NTU-60		
Method	Bones	X-Sub X-View
STA-LSTM [52] (2017)		73.4 81.2
VA-LSTM [53] (2017)		79.4 87.6
AGC-LSTM [54] (2019)		89.2 95.0
ST-GCN [8] (2018)		81.5 88.3
ST-GCN [9]		- 92.7
1s-AGCN [16] [12] (2018)		86.0 93.7
2s-AGCN [16] (2018)	✓	88.5 95.1
DGCNN [9] (2019)	✓	89.9 96.1
1s Shift-GCN [11] (2020)		87.8 95.1
2s Shift-GCN [11] (2020)	✓	89.7 96.0
MS-G3D [12] (2020)	✓	91.5 96.2
SAN [15] (2019)		87.2 92.7
ST-TR		88.7 95.6
ST-TR	✓	<b>89.9 96.1</b>
ST-TR-agcn	✓	89.3 <b>96.1</b>

## VI. COMPARISON WITH STATE-OF-THE-ART RESULTS

In addition to NTU-60, we compare our methods on NTU-120 and Kinetics. On NTU-120, the model based on joint information only, achieves an accuracy of 82.7% on X-Sub and 84.7% on X-Set, outperforming all state-of-the-art methods that use the same information. On Kinetics and NTU-60, we test our model by using also bones information. On Kinetics, our model using only joints outperforms the ST-GCN baseline by 3.8%. When using bones information, the best configuration that uses AGCN instead of GCN (ST-TR-agcn) outperforms the baseline 2s-AGCN by 1.3%, and DGCNN [9] by 0.5%. On NTU-60, our configuration that uses joint information only, outperforms all the state-of-the-art models using the same type of information. In particular, it outperforms SAN [15], which uses self-attention too, by 1.5% on X-Sub and by 2.9% on X-View, and 1s-AGCN by 1.7% on X-Sub and by 1.9% on X-View. The configurations using also bones information outperforms 2s-AGCN by 1.4% on X-Sub, and by 1% on X-View.

Notably, our method is the first one to substitute convolutional modules with fully self-attentional ones, facing the problem of learning long-range correlation with a novel approach. The competitive results validate the superiority of our method over architectures relying on convolution only.

## VII. CONCLUSIONS

In this paper we propose a novel approach that introduces Transformer self-attention in skeleton activity recognition as an alternative to graph convolution. Through extensive experiments on NTU-60, NTU-120 and Kinetics, we demonstrated that our Spatial Self-Attention module (SSA) can replace graph convolution, enabling more flexible and dynamic representations. Similarly, Temporal Self-Attention module (TSA) overcomes the strict locality of standard convolution, leading to global motion pattern extraction. Moreover, our final Spatial-Temporal Transformer network (ST-TR) achieves

state-of-the-art performance on NTU-RGB+D and competitive results on Kinetics with no major hyperparameter tuning.

As combining exclusively self-attention modules revealed to be suboptimal w.r.t. using them separately on two different streams, a possible future work is to search for a fully self-attentional solution, leading to a unified Transformer architecture able to replace graph convolutional networks in a variety of tasks.

APPENDIX  
APPENDIX A  
MODEL COMPLEXITY

In this section we perform an analysis of the complexity of the different self-attention modules we used, compared to the ST-GCN [8] modules based on standard convolution and to the 1s-AGCN [16] modules based on adaptive graph convolution.

*A. Convolution and Transformer blocks*

We analyzed the impact of standard convolution and our novel transformer approach on a single block of  $C_{in} = C_{out}$  channels, by implementing 4 different configurations:

- Graph Convolution (GC): standard graph convolution as in [8]
- Adaptive Graph Convolution (AGC): adaptive graph convolution as in [16]
- Spatial Self-Attention (SSA): our novel Spatial Self-Attention module
- Temporal Convolution (TC): standard temporal convolution as in [8] and in [16]
- Temporal Self-Attention (TSA): our novel Temporal Self-Attention module

The number of parameters of each configuration is shown in Figure 5 as a function of the channel dimension. In both SSA and TSA configurations the *number of heads* for multi-head attention are set to  $N_h = 8$ , the  $d_q$  and  $d_k$  embedding dimensions to  $0.25 \times C_{out}$ , and  $d_v = C_{out}$ . The number of channels is divided equally among the heads, i.e., each head is assigned  $d_h = \frac{d}{N_h}$  channels. Consequently, the *number of heads* used does not influence the total number of parameters. To implement both graph convolution and adaptive graph convolution, we used the *spatial labeling* strategy [8], i.e., nodes are labeled according to their distance with respect to the skeleton gravity center, and 3 partitions of the adjacency matrix are obtained. The same labeling was also used for all the experiments in the paper.

Transformer multi-head attention operates with a  $1 \times stride$  standard  $2D$  convolution on  $C_{in}$  input channels and  $2d_k + d_v$  output channels to calculate query, key, and value, and a  $1 \times 1$   $2D$  convolution combining the output of each head with  $C_{in} = C_{out} = d_v$  input and output channels. This results in the same number of parameters for both Temporal and Spatial Self-Attention, since the convolutions performed internally are the same (having fixed the same kernel dimensions) and both the query-key dot product and the logit-value product are parameter free. Thus, having different input shapes, i.e.,  $T$  (total number of frames) and  $V$  (total number of nodes), does

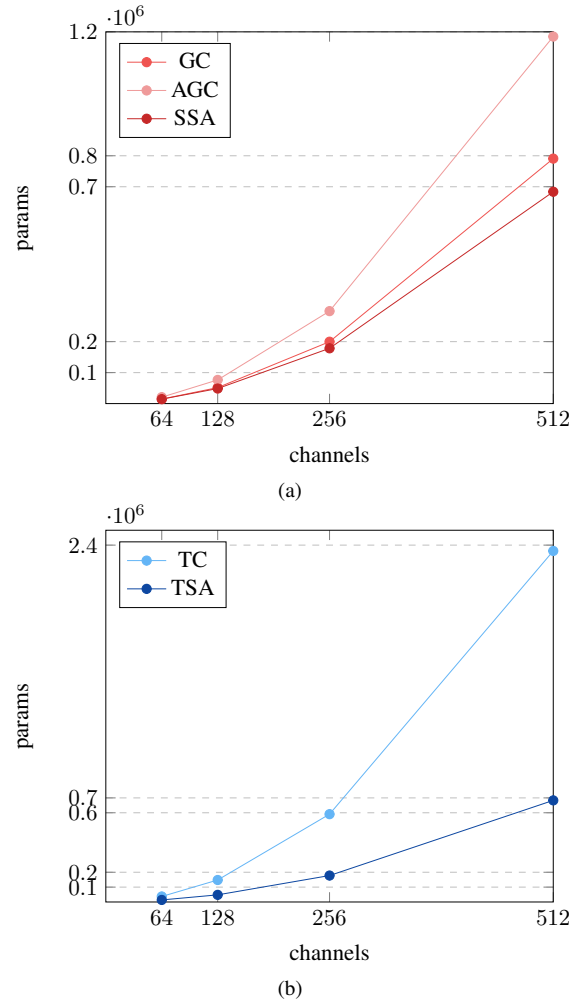


Fig. 5. Difference in terms of parameters (a) between a Graph Convolution module (GC), an Adaptive Convolution module (AGC) and a Spatial Self-Attention module (SSA) of  $C_{in} = C_{out}$  channels, and (b) between a Temporal Convolution module (TC) and a Temporal Self-Attention module (TSA)

not impact on parameters count. The number of parameters introduced by self-attention is then expressed mathematically in Equation 11:

$$TR_{params} = C_{in}C_{out}(2k + v) + C_{out}^2v^2 \quad (11)$$

where  $k = \frac{d_k}{C_{out}} = 0.25$  and  $v = \frac{d_v}{C_{out}} = 1$ .

From Figure 5a it can be seen that Spatial Self-Attention introduces less parameters than graph convolution, especially when dealing with a large number of channels, where the maximum  $\Delta_{GC-SSA}$ , i.e., the decrease in terms of parameters, is  $1.1 \times 10^5$ . Indeed, graph convolution [8] is implemented as a  $1D$  convolution with  $C_{in} = C_{out}$  channels on each adjacency matrix partition  $p_{adj}$ , which is equal to 3 in case of *spatial labeling* [8]. In the case of Spatial Self-Attention most of the model parameters are employed in computing the query and key embeddings, which both use  $0.25 \times C_{out}$  output channels, split among the different heads, compared to graph convolution, which instead makes use

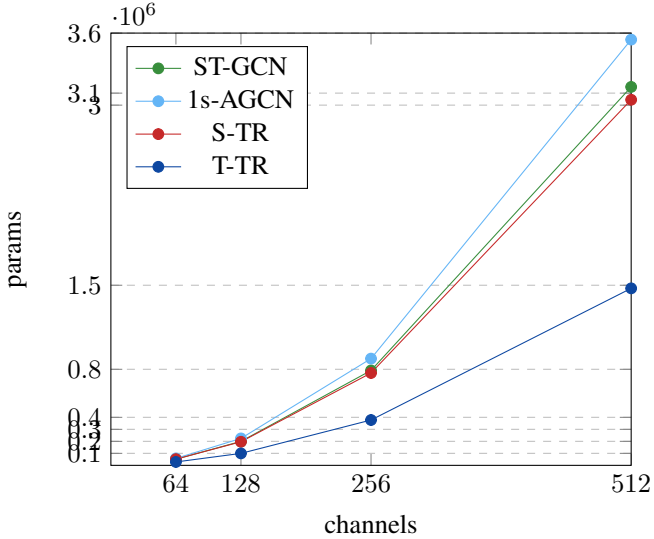


Fig. 6. Comparison in terms of parameters between ST-GCN [8], 1s-AGCN [16] and our novel S-TR and T-TR

of the full  $C_{out}$ , dimension. This decreases significantly the number of parameters in Spatial Self-Attention, especially with large  $C_{out}$ , as demonstrated by Equation 12:

$$\begin{aligned} \Delta_{params} &= C_{in}C_{out} \sum p_{adj} - TR_{params} = \\ &= C_{in}C_{out} \left( \sum p_{adj} - (2k + v) - \frac{C_{out}}{C_{in}}v^2 \right) \end{aligned} \quad (12)$$

When dealing with Adaptive Graph Convolution (AGC), an additional number of parameters has to be considered, which are the ones composing the elements of  $\mathbf{B}_k$ , a matrix whose elements are learned during the training process. This leads to an increase in terms of parameters and thus a difference with respect to SSA of  $\Delta_{AGC-SSA} = 5 \times 10^5$ . On the temporal dimension, Figure 5b,  $\Delta_{TC-TSA}$  reaches a value of  $16.8 \times 10^5$ . Temporal convolution in [8] is implemented as a  $2D$  convolution with filter  $1 \times F$ , where  $F$  is the number of frames considered along the time dimension, and it is usually set to 9, striding along  $T = 300$  frames. Thus, substituting it with a self-attention mechanism results in a great complexity reduction, in addition to better performance. Similarly to the previous analysis, the  $\Delta_{TC-TSA}$  in the temporal dimension can be expressed as it follows:

$$\begin{aligned} \Delta_{params} &= C_{in}C_{out}F - TR_{params} = \\ &= C_{in}C_{out} \left( F - (2k + v) - \frac{C_{out}}{C_{in}}v^2 \right). \end{aligned} \quad (13)$$

### B. Spatial Temporal Transformer and Spatial Temporal Graph Convolution

In this section, we analyze the impact on parameters of combining the modules described in Section A, to compose respectively our Spatial Transformer (S-TR) and Temporal

TABLE V  
TRADE-OFF BETWEEN COMPLEXITY (BOTH IN TERMS OF INFERENCE TIME AND PARAMETERS) AND ACCURACY (%) IN THE BASELINES AND IN OUR TRANSFORMER MODELS

Method	Params $\times 10^5$	Top-1	Top-5	$\Delta_{infer}$
ST-GCN [55]	31.0	92.7	-	-
1s-AGCN	35.0	93.7	-	-
S-TR	30.7	94.0	99.2	+0.2%
T-TR	17.7	93.6	99.1	+0.32%

Transformer (T-TR) streams. In S-TR, either the graph convolution or the adaptive graph convolution is substituted by the Spatial Self-Attention mechanism (SSA), while the temporal convolution is maintained along the time dimension. On the other side, in T-TR the temporal convolution is substituted by the Temporal Self-Attention mechanism (TSA), while the graph convolution is kept along the spatial dimension. The comparison, in terms of parameters, between ST-GCN [8], 1s-AGCN [16], S-TR, and T-TR is shown in Figure 6. As expected from the considerations in Section A, the biggest improvement is achieved by substituting temporal convolution with Temporal Self-Attention, i.e., in T-TR, with a  $\Delta_{ST-GCN-T-TR} = 16.7 \times 10^5$ . On the spatial dimension the difference in terms of parameters is not as pronounced as in temporal dimension, but it is still significant, with a  $\Delta_{ST-GCN-S-TR} = 1.07 \times 10^5$  and  $\Delta_{1s-AGCN-S-TR} = 5.0 \times 10^5$ .

While the previous analysis was performed studying a single block having  $C_{in} = C_{out}$  channels, in the following we perform a complexity analysis on the network configuration used in the paper, i.e., on an architecture of 9 layers with channels that go from 64 to 256 [8]. The trade-off between complexity and performances in terms of accuracy is illustrated in Table V. On the spatial dimension, our model, while having less parameters than the original ST-GCN and 1s-AGCN models, improves Top-1 accuracy by 1.3% and 0.4% respectively. On the temporal dimension, the number of parameters required is half of the ones required for the baseline ST-GCN; nonetheless, the T-TR configuration, despite being lighter, leads to an improvement in performance of 0.9%.

The self-attention mechanism [13] is implemented through matrix multiplications between very large matrices and this leads to more complexity in terms of computational time. Especially on temporal dimension, the query-dot product is computed between a query matrix  $\mathbf{Q}$  of shape  $(N, N_h, T, d_q^h)$  and a key matrix  $\mathbf{K}$  of shape  $(N, N_h, T, d_k^h)$  (more details on the paper), where  $T = 300$  in the very first layers, then  $T = 150$  and finally  $T = 75$ ,  $N_h = 8$  is the number of heads,  $N$  is the batch size and  $dh_q = dh_k$  is the embedding dimension.

The time cost is analyzed in Table V via the variation in percentage of time inference ( $\Delta_{infer}$ ) calculated between the baseline ST-GCN and S-TR and T-TR respectively. As far as concern time complexity, we consider an increment of less than 0.4% acceptable, and we leave further optimizations to

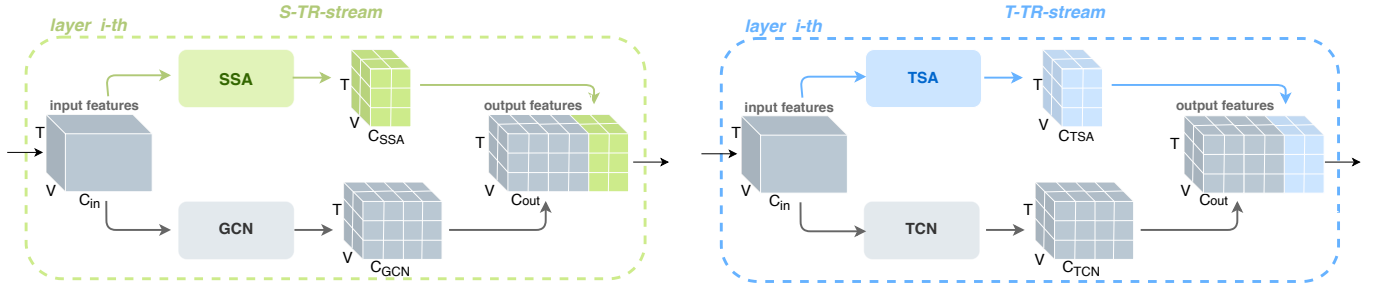


Fig. 7. ST-TR augmented. At each layer, the features resulting from the SSA ( $C_{SSA}$ ) or the TSA ( $C_{TSA}$ ) module, are concatenated to the features resulting from Graph ( $C_{GC}$ ) or Temporal Convolution ( $C_{TC}$ ) respectively along the depth dimension ( $C_{out}$ ).  $V$  indicated the body joint dimension, and  $T$  indicates the temporal dimension.

future works.

## APPENDIX B

### SELF-ATTENTION AS AN AUGMENTATION PROCEDURE TO CONVOLUTION

In this section we provide a detailed description on the configuration that uses self-attention as an augmentation procedure to ST-GCNs, referred in the paper as *ST-TR-augmented* and described in Section V-e.

#### A. Augmented Convolution

In [56], Bello et al. proposed to overcome the locality limitations of standard convolution by augmenting it with the self-attention operator, known to effectively model long-term dependencies. This has been obtained by concatenating features from convolution with features derived from self-attention, as expressed in the following:

$$AACConv(X) = Concat[Conv(X), MHA(X)] \quad (14)$$

where  $\mathbf{X}$  is an input image of shape  $(H, W, F_{in})$ ,  $Conv$  indicates the standard convolution operator, and  $MHA$  indicates Multi-Headed Attention.

#### B. S-TR as an augmentation to ST-GCN

As augmented convolution with self-attention demonstrated to be effective in [56], we performed experiments in a model configuration where SSA and TSA do not substitute completely GCN and TCN respectively, but they are combined with them as a features augmentation mechanism. The process is shown in Figure 7. In this configuration, on S-TR stream,  $0.75 \times C_{out}$  of the output features are obtained by processing the input with GCN, and the remaining  $0.25 \times C_{out}$  features from SSA. The two set of features are then concatenated to build the final output. Similarly, on T-TR stream,  $0.75 \times C_{out}$  features resulting from TCN are concatenated to the remaining  $0.25 \times C_{out}$  features from TSA.

#### C. Implementation

Given an input  $\mathbf{X} \in \mathbb{R}^{C_{in} \times T \times V}$ , where  $C_{in}$  is the number of input features,  $T$  is the number of frames and  $V$  is the number of nodes, on S-TR stream a matrix  $\mathbf{X}_V \in \mathbb{R}^{C_{in} \times 1 \times V}$  is obtained by reshaping the input and moving the  $T$  dimension

inside the batch. Then, a standard graph convolution as in [8] is performed on the input  $\mathbf{X}$ , with  $0.75 \times C_{out}$  features in output. On the other side, input  $\mathbf{X}_V$  is processed by SSA, resulting in  $0.25 \times C_{out}$  features. After reshaping the result by moving out the dimension  $T$ , it is concatenated to the one obtained by convolution on channel dimension. Similarly, on T-TR, an input  $\mathbf{X}_T \in \mathbb{R}^{C_{in} \times 1 \times T}$  is obtained by reshaping  $\mathbf{X}$ , and moving the node dimension  $V$  in the batch. Standard 2D convolution with kernel size  $(1, K_t)$ , where  $K_t$  is the kernel on temporal dimension, is applied on input  $\mathbf{X}$ , resulting in  $0.75 \times C_{out}$  features. These are then concatenated to  $0.25 \times C_{out}$  features resulting from TSA on  $\mathbf{X}_T$ , after having reshaped the self-attention output.

## APPENDIX C

### TRANSFORMER VISUALIZATIONS

In this section, we give some details about the logit attention matrices visualized in the videos attached to the supplementary materials, with the goal of highlighting the interpretability of our novel model.

#### A. Spatial Self-Attention Maps

The videos analyzed in this section represent the evolution of Spatial Self-Attention attention maps along time and its weights. Each video corresponds to an action, whose NTU-RGB+D video is shown on the top right, as in Figure 8, where the action *handshaking* is displayed. In addition, a video showing the evolution of the attention logit heatmaps over all layers is added, as well as a video showing the effect of relative positional encoding.

For each person in the video, and for each frame, the corresponding heatmaps representing the weights of the attention logits of the last layer are drawn, as shown in Figure 8. The heatmaps are  $25 \times 25$  matrices, where each row and each column represents a body joint. An element in position  $(i, j)$  represents the correlation between joint  $i$  and joint  $j$ .

On the top-right portion of the video we draw the skeleton of the subjects, where the radius of the circles is proportional to the joint's relevance. The relevance of each joint is calculated as the sum over columns of the logit attention matrix, i.e., for each joint the total relevance w.r.t. all the other joints.

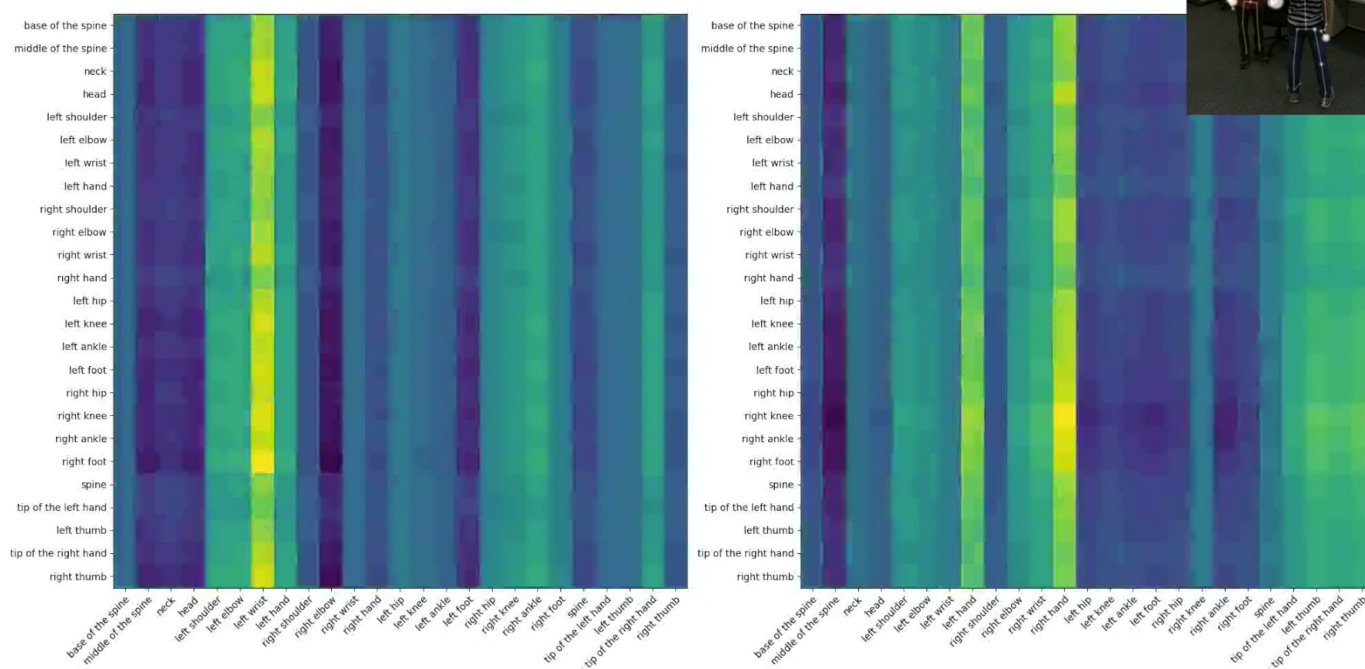


Fig. 8. Screenshot of a frame of our Transformer visualization video for action *handshaking*. Color violet represents the minimum value and yellow the maximum.

### B. Interpretability

A great AI debate of the last years is interpretability [57], the ability of one model to provide reasonable explanations to its decisions. In Skeleton Action Recognition tasks in particular, it is of crucial importance that the model can provide *explanations*, in order to be able to understand what is underlying the recognition of an action, both to see if what is algorithmically learned corresponds to what happens from the human psychology point of view, and for the acceptance of this models in critical applications as security-related ones.

Our novel ST-TR model leads to interpretable results, as the relevance of each joint in classifying an action and correlations between the different body parts are immediately represented in the attention logit matrices. From the heatmaps in Figure 8, it can be seen that the model identifies the most relevant body parts in the action of *handshaking*, represented by the highlighted columns, as the *left wrist* for the person on the left, and *left hand* and *right hand* for the person on the right. Indeed, this is also shown in the RGB+Skeleton video on the top right, where it can be seen that the model focus on the hands that are performing the action.

### REFERENCES

- [1] Z. Zhang, "Microsoft kinect sensor and its effect," *IEEE MultiMedia*, 2012.
- [2] Z. Ren, J. Meng, J. Yuan, and Z. Zhang, "Robust hand gesture recognition with kinect sensor," *Proceedings of the 2011 ACM Multimedia Conference and Co-Located Workshops*, 2011.
- [3] Z. Cao, G. Hidalgo, T. Simon, S. Wei, and Y. Sheikh, "Openpose: Realtime multi-person 2d pose estimation using part affinity fields," *CVPR*, 2017.
- [4] X. Chu, W. Yang, W. Ouyang, C. Ma, A. L. Yuille, and X. Wang, "Multi-context attention for human pose estimation," *CVPR*, 2017.
- [5] H.-B. Zhang, Y.-X. Zhang, B. Zhong, Q. Lei, L. Yang, J.-X. Du, and D.-S. Chen, "A comprehensive survey of vision-based human action recognition methods," *Sensors*, 2019.
- [6] J. Aggarwal and M. Ryoo, "Human activity analysis: A review," *ACM Computing Surveys*, 2011.
- [7] B. Ren, M. Liu, R. Ding, and H. Liu, "A survey on 3d skeleton-based action recognition using learning method," *arXiv*, 2020.
- [8] S. Yan, Y. Xiong, and D. Lin, "Spatial temporal graph convolutional networks for skeleton-based action recognition," *AAAI*, 2018.
- [9] L. Shi, Y. Zhang, J. Cheng, and H. Lu, "Skeleton-based action recognition with directed graph neural networks," *CVPR*, 2019.
- [10] K. Simonyan and A. Zisserman, "Two-stream convolutional networks for action recognition in videos," *CVPR*, 2014.
- [11] K. Cheng, Y. Zhang, X. He, W. Chen, J. Cheng, and H. Lu, "Skeleton-based action recognition with shift graph convolutional network," *CVPR*, 2020.
- [12] Z. Liu, H. Zhang, Z. Chen, Z. Wang, and W. Ouyang, "Disentangling and unifying graph convolutions for skeleton-based action recognition," June 2020.
- [13] A. Vaswani, N. Shazeer, N. Parmar, J. Uszkoreit, L. Jones, A. N. Gomez, L. Kaiser, and I. Polosukhin, "Attention is all you need," *NIPS*, 2017.
- [14] I. Bello, B. Zoph, A. Vaswani, J. Shlens, and Q. V. Le, "Attention augmented convolutional networks," *ICCV*, 2019.
- [15] S. Cho, M. Maqbool, F. Liu, and H. Foroosh, "Self-attention network for skeleton-based human action recognition," 2020.
- [16] L. Shi, Y. Zhang, J. Cheng, and H. Lu, "Two-stream adaptive graph convolutional networks for skeleton-based action recognition," *CVPR*, 2018.
- [17] J.-F. Hu, W.-S. Zheng, J.-H. Lai, and J. Zhang, "Jointly learning heterogeneous features for rgb-d activity recognition," *IEEE Transactions on Pattern Analysis and Machine Intelligence*, 2016.

- [18] R. Vemulapalli, F. Arrate, and R. Chellappa, "Human action recognition by representing 3d human skeletons as points in a lie group," *CVPR*, 2014.
- [19] M. Hussein, M. Torki, M. Gowayed, and M. El Saban, "Human action recognition using a temporal hierarchy of covariance descriptors on 3d joint locations," *IJCAI International Joint Conference on Artificial Intelligence*, 2013.
- [20] L. Wang, D. Huynh, and P. Koniusz, "A comparative review of recent kinect-based action recognition algorithms," *IEEE Transactions on Image Processing*, 2019.
- [21] G. Lev, G. Sadeh, B. Klein, and L. Wolf, "Rnn fisher vectors for action recognition and image annotation," *ECCV*, 2015.
- [22] H. Wang and L. Wang, "Modeling temporal dynamics and spatial configurations of actions using two-stream recurrent neural networks," *CVPR*, 2017.
- [23] J. Liu, G. Wang, P. Hu, L.-Y. Duan, and A. C. Kot, "Global context-aware attention lstm networks for 3d action recognition," *CVPR*, 2017.
- [24] Y. Du, W. Wang, and L. Wang, "Hierarchical recurrent neural network for skeleton based action recognition," *CVPR*, 2015.
- [25] G. Chéron, I. Laptev, and C. Schmid, "P-cnn: Pose-based cnn features for action recognition," *ICCV*, 2015.
- [26] K. Simonyan and A. Zisserman, "Two-stream convolutional networks for action recognition in videos," *NIPS*, 2014.
- [27] Z. Ding, P. Wang, P. Ogunbona, and W. Li, "Investigation of different skeleton features for cnn-based 3d action recognition," *ICME*, 2017.
- [28] M. Liu, H. Liu, and C. Chen, "Enhanced skeleton visualization for view invariant human action recognition," *Pattern Recognition*, 2017.
- [29] B. Li, Y. Dai, X. Cheng, H. Chen, Y. Lin, and M. He, "Skeleton based action recognition using translation-scale invariant image mapping and multi-scale deep cnn," *ICMEW*, 2017.
- [30] M. M. Bronstein, J. Bruna, Y. LeCun, A. Szlam, and P. Vandergheynst, "Geometric deep learning: going beyond euclidean data," *IEEE Signal Processing Magazine*, 2016.
- [31] M. Gori, G. Monfardini, and F. Scarselli, "A new model for learning in graph domains," *Proceedings. 2005 IEEE International Joint Conference on Neural Networks*, 2005.
- [32] F. Scarselli, M. Gori, A. C. Tsoi, M. Hagenbuchner, and G. Monfardini, "The graph neural network model," *IEEE Transactions on Neural Networks*, pp. 61–80, 2009.
- [33] J. Bruna, W. Zaremba, A. Szlam, and Y. Lecun, "Spectral networks and locally connected networks on graphs," *ICLR*, 2014.
- [34] M. Henaff, J. Bruna, and Y. LeCun, "Deep convolutional networks on graph-structured data," *NIPS*, 2015.
- [35] M. Defferrard, X. Bresson, and P. Vandergheynst, "Convolutional neural networks on graphs with fast localized spectral filtering," *NIPS*, 2016.
- [36] T. N. Kipf and M. Welling, "Semi-Supervised Classification with Graph Convolutional Networks," *ICLR*, 2017.
- [37] A. Micheli, "Neural network for graphs: A contextual constructive approach," *IEEE Transactions on Neural Networks*, 2009.
- [38] M. Niepert, M. Ahmed, and K. Kutzkov, "Learning convolutional neural networks for graphs," *International conference on machine learning*, 2016.
- [39] F. P. Such, S. Sah, M. Domínguez, S. Pillai, C. Zhang, A. Michael, N. D. Cahill, and R. W. Ptucha, "Robust spatial filtering with graph convolutional neural networks," *IEEE Journal of Selected Topics in Signal Processing*, 2017.
- [40] Y. Li, X. Liang, Z. Hu, Y. Chen, and E. P. Xing, "Graph transformer," *OpenReview*, 2019.
- [41] S. Ioffe and C. Szegedy, "Batch normalization: Accelerating deep network training by reducing internal covariate shift," *arXiv*, 2015.
- [42] T. Q. Nguyen and J. Salazar, "Transformers without tears: Improving the normalization of self-attention," *arXiv*, 2019.
- [43] A. Shahroudy, J. Liu, T. Ng, and G. Wang, "NTU RGB+D: A large scale dataset for 3d human activity analysis," *CVPR*, 2016.
- [44] W. Kay, J. Carreira, K. Simonyan, B. Zhang, C. Hillier, S. Vijayanarasimhan, F. Viola, T. Green, T. Back, A. Natsev, M. Suleyman, and A. Zisserman, "The kinetics human action video dataset," *ArXiv*, 2017.
- [45] J. Liu, A. Shahroudy, M. Perez, G. Wang, L.-Y. Duan, and A. Kot, "Ntu rgb+d 120: A large-scale benchmark for 3d human activity understanding," *IEEE Transactions on Pattern Analysis and Machine Intelligence*, 2019.
- [46] A. Paszke, S. Gross, F. Massa, A. Lerer, J. Bradbury, G. Chanan, T. Killeen, Z. Lin, N. Gimelshein, L. Antiga *et al.*, "Pytorch: An imperative style, high-performance deep learning library," in *Advances in Neural Information Processing Systems*, 2019.
- [47] Z. Lin, P. Liu, L. Huang, J. Chen, X. Qiu, and X. Huang, "Dropattention: A regularization method for fully-connected self-attention networks," *ArXiv*, 2019.
- [48] J. Liu, A. Shahroudy, D. Xu, and G. Wang, "Spatio-temporal LSTM with trust gates for 3d human action recognition," *ECCV*, 2016.
- [49] J. Liu, G. Wang, L. Duan, K. Abdiyeva, and A. C. Kot, "Skeleton-based human action recognition with global context-aware attention lstm networks," *IEEE Transactions on Image Processing*, 2017.
- [50] Q. Ke, M. Bennamoun, S. An, F. Sohel, and F. Boussaid, "Learning clip representations for skeleton-based 3d action recognition," *IEEE Transactions on Image Processing*, 2018.
- [51] M. Liu and J. Yuan, "Recognizing human actions as the evolution of pose estimation maps," *CVPR*, 2018.
- [52] S. Song, C. Lan, J. Xing, W. Zeng, and J. Liu, "An end-to-end spatio-temporal attention model for human action recognition from skeleton data," *AAAI*, 2016.
- [53] P. Zhang, C. Lan, J. Xing, W. Zeng, J. Xue, and N. Zheng, "View adaptive recurrent neural networks for high performance human action recognition from skeleton data," *ICCV*, 2017.
- [54] C. Si, W. Chen, W. Wang, L. Wang, and T. Tan, "An attention enhanced graph convolutional lstm network for skeleton-based action recognition," *CVPR*, 2019.
- [55] L. Shi, Y. Zhang, J. Cheng, and H. Lu, "Skeleton-based action recognition with directed graph neural networks," *CVPR*, 2019.
- [56] I. Bello, B. Zoph, A. Vaswani, J. Shlens, and Q. V. Le, "Attention augmented convolutional networks," *ICCV*, 2019.
- [57] L. H. Gilpin, D. Bau, B. Z. Yuan, A. Bajwa, M. Specter, and L. Kagal, "Explaining explanations: An approach to evaluating interpretability of machine learning," *IEEE 5th International Conference on Data Science and Advanced Analytics (DSAA)*, 2018.